



HAL
open science

Induced anisotropic gas permeability of concrete due to coupled effect of drying and temperature

Mohamad Ezzedine El Dandachy, Matthieu Briffaut, Stefano Dal Pont,
Frédéric Dufour

► **To cite this version:**

Mohamad Ezzedine El Dandachy, Matthieu Briffaut, Stefano Dal Pont, Frédéric Dufour. Induced anisotropic gas permeability of concrete due to coupled effect of drying and temperature. *Key Engineering Materials*, 2016, 711, pp.871-878. 10.4028/www.scientific.net/KEM.711.871 . hal-01876933

HAL Id: hal-01876933

<https://hal.science/hal-01876933>

Submitted on 23 Apr 2024

HAL is a multi-disciplinary open access archive for the deposit and dissemination of scientific research documents, whether they are published or not. The documents may come from teaching and research institutions in France or abroad, or from public or private research centers.

L'archive ouverte pluridisciplinaire **HAL**, est destinée au dépôt et à la diffusion de documents scientifiques de niveau recherche, publiés ou non, émanant des établissements d'enseignement et de recherche français ou étrangers, des laboratoires publics ou privés.

Induced Anisotropic Gas Permeability of Concrete due to Coupled effect of Drying and Temperature

Mohamad EZZEDINE EL DANDACHY*, Matthieu BRIFFAUT,
Stefano DAL PONT and Frederic DUFOUR

Univ. Grenoble Alpes, 3SR, F-38000 Grenoble, France
CNRS, 3SR, F-38000 Grenoble, France

E-mail: mohamad.ezzedineeldandachy@3sr-grenoble.fr,
web page: www.3sr-grenoble.fr

Keywords: thermal loading, drying shrinkage, gas permeability, longitudinal/radial, concrete.

Abstract. An experimental campaign is carried out to study the effect of drying shrinkage and temperature on multi-directional gas permeability of dry concrete. Thermal loadings up to 250°C are applied on concrete samples in cylinder (11×22) and dog-bone forms (total length of 61 cm). Samples are sliced for permeability measurements. Permeabilities in longitudinal and radial directions are addressed. The cylinder samples are first sliced then dried or heated whilst the dog-bone samples are first dried or heated then sliced. The average of initial intrinsic permeability for the slices (5 cm height, 11 cm diameter) obtained from the (11×22) samples is found isotropic and equal to 2.93×10^{-17} m². In this case, drying shrinkage is isotropic. Furthermore, it is shown that for the dog-bone samples, drying shrinkage may induce micro-cracks preferentially in a certain direction which induces permeability anisotropy. Finally, the evolution of the normalized intrinsic permeability with respect to initial permeability versus temperature is found isotropic. An exponential fitting of intrinsic permeability versus temperature is found based on experimental measurements.

Introduction

During a severe accident such as a LOCA (Loss Of Coolant Accident in nuclear power plant) scenario, temperature in the pre-stressed concrete containment rises up to 180°C and the pressure may reach 5 bars which leads to thermo-hygro-mechanical stresses that cause the appearance of cracks. This accident may last for two weeks which also generates thermally activated creep. The overall leakage rate of a heavily reinforced and pre-stressed concrete structure is governed by the concrete gas permeability which is strongly dependent on the thermo-mechanical and hydric state.

Before the appearance of a localized crack, transport phenomena are governed by the porous network of the cementitious material and its degree of saturation. Drying shrinkage creates micro-cracks in concrete which alter the initial porous network and lead to permeability increase. This latter may induce permeability anisotropy in concrete structure depending on its geometry; for instance in walls longitudinal permeability is more significant than transversal one [1]. Furthermore, the temperature rise (above 140 °C) causes the departure of water that is chemically bounded to the hydrates of concrete [2, 3, 4], also amending its porous network (and its mechanical behavior) and could highly increase the gas permeability of concrete [5, 6]. In addition to the changes in the intrinsic properties of the cement paste, micro-cracks may be generated by the interaction between aggregates and cement paste as these two components have different thermal expansions and different stress-strain relationships [7]. Consequently, micro-cracks of different origins should be taken into account in the estimation of the intrinsic permeability of concrete. When a macro-crack appears due to micro-cracks coalescence, it becomes a preferential channel for the fluid and almost all of the leakage flows through this macro-crack [8, 9, 10].

Studies in the literature have shown that the evolution of gas permeability of concrete is found to be exponential (or power law) with respect to temperature [11, 12]. The effect of temperature on water

permeability of ordinary concrete as well as the correlation on experimental tests was determined in [12]. However, the evolution of gas permeability with respect to temperature for this particular concrete, representative of the use in nuclear industry, has to be determined first experimentally to identify the permeability-temperature correlation. Finally, the isotropic/anisotropic property of permeability of samples in cylindrical and dog-bone forms due to drying shrinkage and temperature will be studied.

Experimental Campaign

Concrete Formulation

The concrete studied in this contribution is the reference concrete for the national project MaCEnA (tightness assessment of confinement vessels during an accident). The compressive strength of this concrete is around 45 MPa at 28 days. The Young's Modulus is around 40 GPa at ambient temperature. The different constituents and their quantities are given in table 1.

Table 1: Formulation of MaCEnA's concrete.

Constituents	Quantity (kg/m ³)
CEM I 52.5 N CE CP2 NF "GAURAIN"	320
Sand calcium silicates 0/4 Reconstuted mix LGP1 "GSM" 0/4	830
Gravels calcium silicates 4/11 LGP1 "GSM"	445
Gravels calcium silicates 4/11 BALLOY "GSM"	550
Admixture SIKAPLAST TECHNO 80	2.4
Water	197.5

Gas Permeability Device

A general view of the permeability device is presented in Fig. 1. It is composed of:

- 1) Three mass flowmeters with different measuring range, the highest 25000 mln/min, the intermediate 750 mln/min and the lowest 20 mln/min. (n: normal conditions; 0°C, 1 atm)
- 2) Pressure regulator that controls accurately the gas pressure.
- 3) Gas reservoir of nitrogen (N₂) provided with a pressure reducer.
- 4) The impervious containment (see Fig. 2 for details). Note that the specimen holder is replaceable to fit with the specimen.
- 5) A PC for data acquisition.

This permeability device gives the possibility of testing concrete permeability in both longitudinal and radial directions thanks to the mechanical system shown in Fig. 2a. The configurations for the permeability test in longitudinal and radial direction are presented respectively in Fig. 2b and Fig. 2c. For practical purposes and due to technical limitations, the study is limited to residual permeability of completely dried specimens. Each permeability measurement is performed under controlled gas pressure ranged from 1.5 to 3.5 bars.

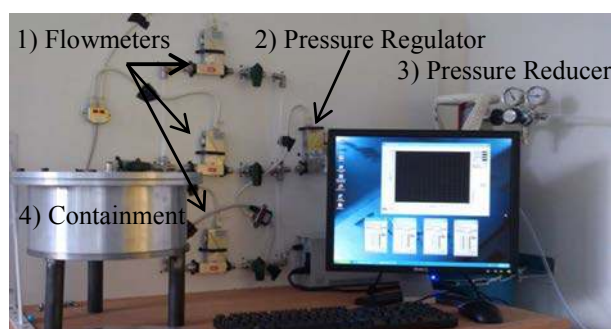


Fig. 1: Permeameter device

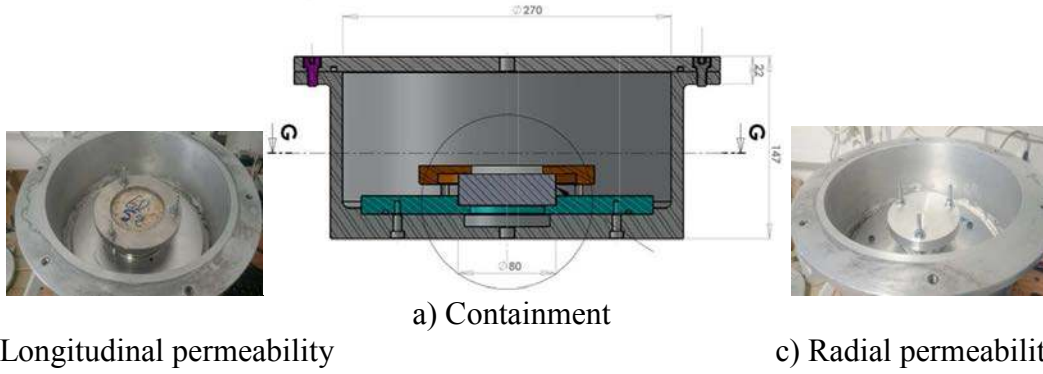


Fig. 2: Technical draws of the containment (a), longitudinal permeability testing (b) and radial permeability testing (c).

Permeability Estimation

The permeability test is performed by injecting gas in the containment under a given pressure. Boundary conditions using aluminum foils are imposed on the samples to impose the percolation path, e.g. aluminum foil is placed on the lateral surface of the sample for the longitudinal configuration (see Fig. 2b) whilst it is placed on the flat surfaces for the radial configuration (see Fig. 2c).

After verifying that the regime is laminar, the longitudinal apparent permeabilities are calculated using Darcy's law [13] for compressible fluids (Nitrogen) (Eq. 1) and similarly for the radial apparent permeabilities (Eq. 2)

$$k_{al} = \frac{Q_i^l}{S} \frac{2\mu L P_{atm}}{(P_i^2 - P_{atm}^2)} \quad (1)$$

$$k_{ar} = \frac{Q_i^r}{\pi L} \frac{\mu \ln\left(\frac{r_2}{r_1}\right) P_{atm}}{(P_i^2 - P_{atm}^2)} \quad (2)$$

Where Q_i^l and Q_i^r are the inlet flow rates in the longitudinal and radial direction respectively. They are measured using the mass flowmeters and expressed in mln/min. Note that since the flowmeters are mass ones, the measured flowrates are given under normal conditions and therefore P_{atm} (1.013 bar) must be used in Eq. (1) and (2). Moreover, μ is the dynamic viscosity of N_2 at 20°C, P_i is the gas pressure at the inlet and r_1, r_2, L and S are geometrical parameters.

Thermal loading on samples

Cylindrical samples of MaCEnA's concrete were casted and tested in laboratory 3SR, other dog-bone samples (same concrete) were casted and tested in the technical center CERIB. All samples were conserved and cured following Rilem Tc 129 recommendations [14].

Nine Slices (50 mm height and 110 mm diameter) of three concrete samples (3 slices per sample) whose dimensions are 11×22 cm (cylindrical), are conducted for temperature tests. Five are used for longitudinal permeability measurements and four others (drilled, hole of 16 mm diameter) for radial permeability measurements. It should be noted that the thermal loading is applied to the slices and not to the entire 11×22 samples. The slices are dried first at 80°C until their mass stabilization before determining their reference permeability. Concerning the application of the thermal loading, the slices are heated under the desired temperature (80°C to 250°C) until the mass stabilization (heating rate is 1°C/min). The permeability measurements are performed in the unloaded state at room temperature after cooling down.

Three dog-bone samples were casted for initial permeability measurements. After slicing, 9 slices (40 mm height, 80 mm diameter) were used to determine the initial intrinsic permeability in both

directions. Permeability test in longitudinal direction is performed first. Then slices are drilled (16 mm hole) for radial permeability tests (one is kept undrilled for longitudinal permeability measurement at different temperatures). Later on, those slices are conducted to temperatures tests up to 220 °C. In this case, thermal loading is applied to slices. Plus, for temperatures 100 °C and 180 °C, one dog-bone sample is prepared each (see Fig. 3a). In this case, temperature is applied to the whole sample (slicing comes after temperature tests). The dog-bone form is chosen because similar samples will be used in another study for thermo-mechanical loading (thermal and traction creep), and with this geometry the traction stress will be equally distributed in the central part of the sample. Furthermore, it is interesting to study the effect of sample geometry on drying shrinkage which affects the permeability in both directions. Temperature is maintained for two weeks. All unheated slices are dried at 80°C until their mass stabilization before the permeability tests.

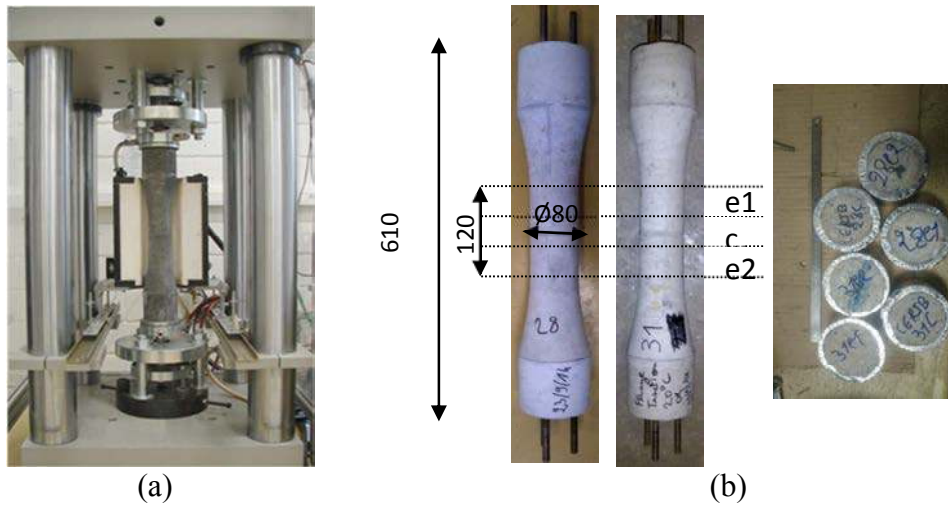


Fig. 3: (a) Experimental set-up for delayed thermo-mechanical tests (b) Concrete slices for permeability tests.

Klinkenberg’s Effect

It is well known that Darcy’s law for compressible gases applied to concrete overestimates the intrinsic permeability, thus to find an intrinsic permeability of concrete Klinkenberg correction is adopted [15]. It consists of performing permeability tests on concrete sample with different gas pressures leading to different apparent permeabilities. Then, by plotting the apparent permeabilities versus the inverse of the mean gas pressure, a linear fit is found if the flow is laminar. The linear regression of the fitted line until it intersects with the y-axis (infinite gas pressure) gives the intrinsic permeability of the sample. Klinkenberg corrections for three slices and for two temperatures are presented in Fig. 4. It is shown that hypothesis for the Klinkenberg correction is checked. Moreover, between two temperatures, it is shown that the apparent permeabilities increase as well as the slope of Klinkenberg regression line.

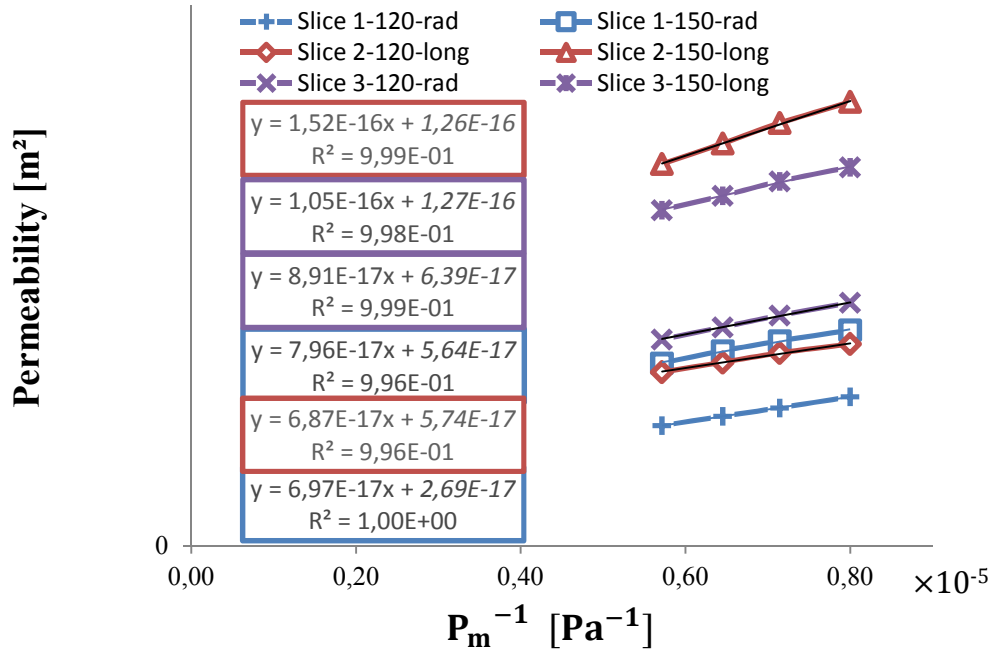


Fig. 4: Klinkenberg correction for concrete samples.

Intrinsic Permeability

Initial Permeability

The initial reference permeability is considered as the permeability measured after applying 80°C. It is averaged on 9 slices (50 mm height, 110 mm diameter) of 11×22 cm samples. The obtained average intrinsic permeability is equal to 2.93×10^{-17} m². Moreover, permeabilities in both directions, longitudinal and radial, are found exactly equal. It means that the effect of drying shrinkage on the intrinsic permeability for those concrete slices (50 mm height, 110 mm diameter) is isotropic. However, the permeability tests performed on slices (40 mm height, 80 mm diameter) from the dog-bone samples have given an average intrinsic permeability of 7.17×10^{-17} m² in the longitudinal direction and 4.49×10^{-17} in the radial direction. Longitudinal permeability is higher than the one in radial direction, thus a slight anisotropy is found. It should be mentioned that drying shrinkage has occurred on the whole dog-bone sample. As discovered in [1], micro-cracks occur first preferentially along the direction that corresponds to the highest drying gradient (radial/transverse direction) induced by the sample/structure geometry (long dog-bone samples). In a second time, the opening, the length and the connectivity of the cracks become more important and lead to an increase in the longitudinal permeability. As for the radial permeability, micro-cracks do not completely cross the sample, which provides lower permeability. Nevertheless, this induced anisotropy is relatively slight when the sample is unloaded.

Temperature effect on gas permeability of concrete

Effect of temperature on concrete residual intrinsic permeability in both directions, longitudinal and radial, is addressed in this subsection. Interest is given particularly to temperatures up to 250 °C. This study is performed on 11×22 cm cylindrical and dog-bone (see Fig. 3b) samples. Each sample was cut into slices (50 mm height, 110 mm diameter) for permeability measurements. See section (“Thermal loading on samples”) for test procedure. For those samples the average of the initial intrinsic permeability is found isotropic and equal to 2.93×10^{-17} m². The evolutions of the normalized intrinsic permeability in both directions versus temperature are presented in Fig. 5. It shows that the concrete residual permeability increases exponentially with the increase of

temperature. This result is in agreement with studies in [5, 11, 12]. Furthermore, the result shown in Fig. 5 shows that normalized intrinsic permeabilities of those slices remain isotropic after temperature tests. It means that the thermal degradation in those slices is isotropic. It should be noted that at 250 °C, the concrete intrinsic permeability has increased of one order of magnitude with respect to the initial intrinsic permeability.

Seen that intrinsic permeability is isotropic with respect to temperature, one exponential fitting, valid in longitudinal and radial directions, is proposed. It is given in Eq. 3.

$$\frac{k_T}{k_0} = e^{C_T(T-T_0)} \quad (3)$$

Where k_T (m^2) is the residual intrinsic permeability after cooling from temperature T (°C) and k_0 is the intrinsic permeability at T_0 (80°C). The concrete parameter C_T is found equal to 0.0158 (°C) $^{-1}$. The parameter C_T found in this study is very comparable to the ones found in the study of temperature effect on water intrinsic permeability of high performance concretes (HPCs) at elevated temperatures (200 °C to 700°C). The parameters C_T found for C60, C60 SF, C70 and C90 are equal to 0.0144, 0.012, 0.011 and 0.02 respectively.

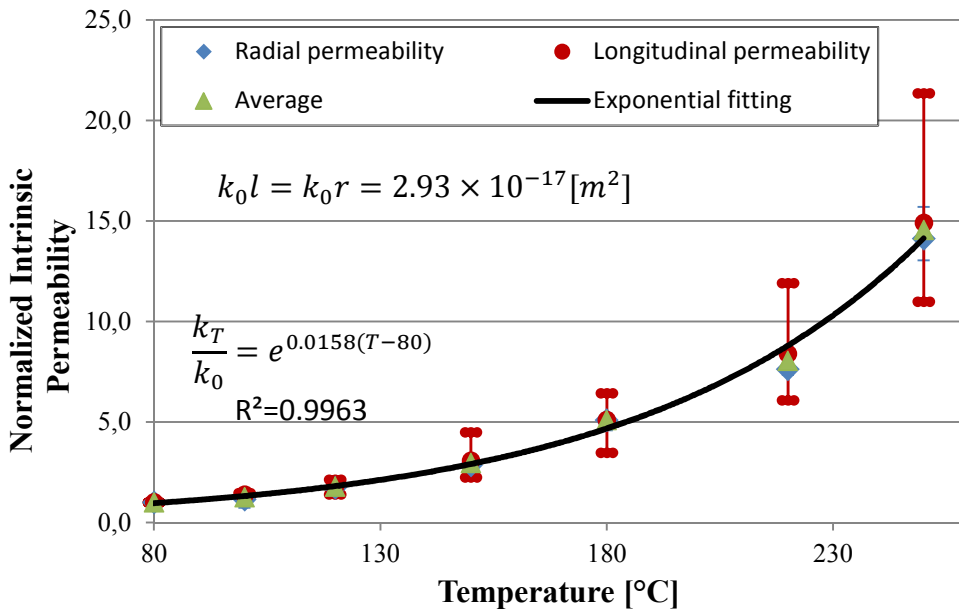


Fig. 5: Evolution of the normalized intrinsic permeability versus temperature (slices from 11×22 concrete samples).

As for the dog-bone samples, an average ratio between longitudinal and radial initial permeability of 1.6 is found. Thus, to better compare the permeability evolutions in both directions, the normalized intrinsic permeability is addressed. Note that for temperatures 100 and 180 °C, one dog-bone sample is tested per temperature. Unfortunately, for practical reasons within the MaCEnA project, the initial intrinsic permeabilities could not be assessed for those samples. However, three unloaded dog-bone samples (9 slices) were used to determine the initial intrinsic permeability in both directions. This procedure of normalization certainly is not perfect but allows us to better compare the intrinsic permeabilities in both directions. The normalized intrinsic permeability versus temperature is presented in Fig. 6. It shows that the normalized intrinsic permeability is almost isotropic and increases exponentially with the increase of temperature. The slight difference between longitudinal and radial normalized permeabilities at 180 °C and 220 °C could be due to normalization error. Finally, the parameter C_T is found equal to 0.0136 and 0.013 (°C) $^{-1}$ for the radial and longitudinal directions respectively.

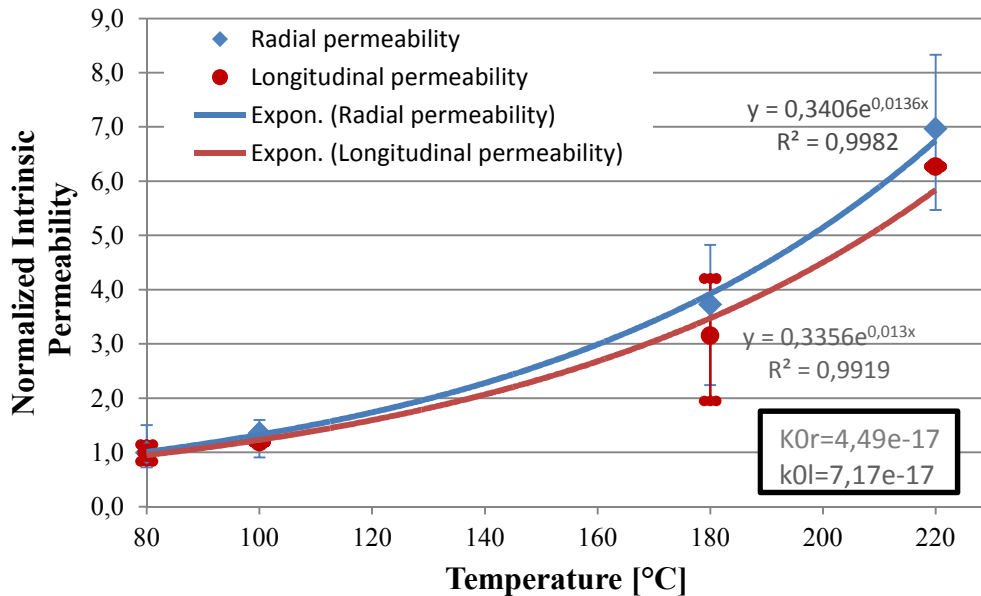


Fig. 6: Evolution of the normalized intrinsic permeability versus temperature (slices from dog-bone concrete samples).

Conclusions

In this contribution, drying shrinkage and temperature effects on intrinsic permeability of concrete in two directions, longitudinal and radial, are analyzed. Initial intrinsic permeability of MaCEnA's concrete is found isotropic and equal to $2.93 \times 10^{-17} \text{ m}^2$. In some cases, based on sample geometry, drying shrinkage may induce micro-cracks preferentially in a certain direction which induce permeability anisotropy. Nevertheless, this anisotropy of drying origin is relatively slight. It was shown that the concrete intrinsic permeability (measured after cooling) increases exponentially with the increase of temperature and in an isotropic manner. The parameter C_T for MaCEnA's concrete is obtained after fitting an exponential function with experimental data.

Acknowledgements

The authors gratefully acknowledge the funding support from France's National Research Agency through "MACENA" project (ANR-11-RSNR-012). 3SR is part of the LabEx Tec 21 (Investissements d'Avenir – Grant agreement no. ANR-11-LABX-0030).

References

- [1] N. Burlion, F. Skoczylas, T. Dubois. Induced anisotropic permeability due to drying of concrete. *Cement and Concrete Research*, Elsevier (2003). 33 (5) 679-687.
- [2] V. Baroghel-Bouny, *Caractérisation des pâtes de ciment et des bétons; méthodes, analyse, interprétations*, Edition du Laboratoire Central des Ponts et Chaussées, Paris, 1994.
- [3] U. Diederichs, U. M. Jumppanen, V. Penttala, *Behaviour of high strength concrete at high temperature*, Espoo: Helsinki University of Technology, Report 92, 1989.
- [4] A. Noumowé, *Effet de hautes températures (20-600 °C) sur le béton. Cas particulier du béton à hautes performance*, Thèse de Doctorat, INSA Lyon, 1995.
- [5] M. Choiniska, A. Khelidj, G. Chatzigeorgiou, G. Pijaudier-Cabot. Effects and interactions of temperature and stress-level related damage on permeability of concrete. *Cement and Concrete Research* (2007). 37 (1) 79–88.

- [6] M. Zeiml, R. Lackner, D. Leithner and J. Eberhardsteiner, Identification of residual gas-transport properties of concrete subjected to high temperatures. *Cement and Concrete Research* (2008). 38(5) 699–716.
- [7] F. Grondin, H. Dumontet, A. Ben Hamida and H. Boussa. Micromechanical contributions to the behaviour of cement-based materials: Two-scale modelling of cement paste and concrete in tension at high temperatures, *Cement and concrete composites* (2010). 33(3) 424-435.
- [8] V. Picandet, A. Khelidj, B. Hervé. Crack effects on gas and water permeability of concretes. *Cement and Concrete Research* (2009). 39(6) 537-47.
- [9] A. Akhavan, S. Seyed-Mohammad-Hadi and R. Farshad. Quantifying the effects of crack width, tortuosity, and roughness on water permeability of cracked mortars. *Cement and Concrete Research* (2012); 42(2) 313-20.
- [10] G. Rastiello, C. Boulay, S. Dal Pont, JL Tailhan, P. Rossi. Real-time water permeability evolution of a localized crack in concrete under loading. *Cement and Concrete Research* (2014). 56 20-28.
- [11] Z. P. Bazant and W. Thonghutai, Pore pressure and drying of concrete at high temperature, *J. Eng. Mech. Div. ASCE* (1978). 104 1059-1079.
- [12] D. Gawin, C. Alonso, C. Andrade, C. E. Majorana and F. Pesavento, Effect of damage on permeability and hygro-thermel behaviour of HPCs at elevated temperatures: Part 1. Experimental results, *Computers and Concrete* (2005). 2(3) 189-202.
- [13] H. Darcy. *Les Fontaines Publiques de la Ville de Dijon*. Dalmont, Paris. 647 p. & atlas, 1856.
- [14] RILEM TC 129-MHT, Test methods for mechanical properties of concrete at high temperatures, Part 1 Introduction, Part 2 Stress-strain relation, Part 3 Compressive strength, Part 4 Tensile strength, Part 5 Modulus of elasticity, Part 6 Thermal strain, Part 7 Transient creep, Part 8 Steady-state creep, Part 9 Shrinkage, Part 10 Restraint, Part 11 Relaxation.
- [15] L. J. Klinkenberg, The permeability of porous media to liquid and gaz, *American Petroleum Institute, Drilling and Production Practice*, 1941, pp. 200-213.